JOURNAL OF SPACECRAFT AND ROCKETS
Vol. 48, No. 2, March–April 2011

Charging Behavior of Polyimide/Adhesive Components During Eclipse Events in Geostationary Environment

T. Paulmier and B. Dirassen
ONERA, 31055 Toulouse Cedex 4, France
and
D. Payan
Centre National d'Etudes Spatiales, 31041 Toulouse Cedex 9, France

DOI: 10.2514/1.49473

This paper presents an experimental and numerical study carried out in the SIRENE irradiation test facility, installed at ONERA (Toulouse, France), on stacked polyimide/adhesive structures used on solar panels. This study aims at following the evolution of the charging potential built up at the surface of these structures during an eclipse event in geostationary orbit. The samples have therefore been irradiated with a distributed electron spectrum (from 0 to 400 keV). During a first stage, the samples are submitted to light radiation at 293 K. In a second stage (eclipse phase), the electron irradiation is performed in darkness and with a decreasing temperature (down to 113 K). In a final stage (eclipse exit), the samples are submitted to light radiation with an increasing temperature (up to 293 K). We have been able to demonstrate that these solar structures are highly sensitive to temperature and light radiation since the volume conductivity of polyimide films and epoxy adhesives is submitted to noticeable variation with these operative parameters. The major conclusion is that this kind of polyimide/adhesive structure potentially used on solar panels may have to cope with elevated charging potential, which can be highly hazardous especially at the eclipse exit when the solar panel regains its power.

Nomenclature

d_{ad}	=	adhesive width, m
d_{fibres}	=	distance between two adjacent carbon fibers, m
E	=	electric field, V.m^{-1}
e	=	electron charge, $1.6 \cdot 10^{-19}$ C
e_{ad}	=	adhesive thickness, m
$e_{\perp}$	=	thickness of polyimide film, m
I	=	electric current, A
J	=	current density, A.m^{-2}
me	=	electron mass, $9.1\,10^{-31}$ kg
R_{ad}	=	volume resistance of the adhesive film, Ω
R_{sq}	=	sheet resistance, Ω/sq
$R_{//}$	=	surface resistance, Ω
$R_{\perp}$	=	volume resistance related to the polyimide film, Ω
V	=	electric charging potential at the surface of the sample, V
V_{lim}	=	electric charging potential during stationary state in phase 1, V
x	=	abscissa along the square element, m
ε	=	relative dielectric permittivity
ε_0	=	vacuum dielectric permittivity, $=8.85\,10^{-12}$ A$^2 \cdot$ s$^4 \cdot$ kg$^{-1} \cdot$ m^{-3}
ξ	=	incident electron energy, J
ξ_0	=	initial incident electron energy, J
$\rho_{\perp}$	=	volume resistivity of polyimide, Ω.m
ρ_{ad}	=	volume resistivity of epoxy adhesive, Ω.m
σ	=	volume conductivity, Ω^{-1}.m^{-1}
υ	=	electron velocity, m.s^{-1}

Subscripts

H	=	linked to high-density fibers sample
L	=	linked to high-density fibers sample

Received 19 February 2010; revision received 17 August 2010; accepted for publication 8 September 2010.

I. Introduction

FORMER studies [1–4] carried out on space used raw polyimide material have revealed that this kind of material presents a fairly low charging level under geostationary environment thanks to the increased conductivity induced by electron and photon radiation. These features are still observed at low temperature. Charging behavior can, however, be drastically different for real polyimide/adhesive structures used on solar panels, especially during eclipse events. The reason is that epoxy adhesives have to cope with a steep drop of their electric conductivity with the applied decreasing temperature. In the current study, polyimide/adhesive solar panel structures have been tested in the SIRENE irradiation chamber, installed at ONERA (Toulouse, France), which allowed the radiation (electron and photon flux) and thermal simulation of an eclipse event under geostationary environment for a solar magnetic activity K_p higher than five (see Sec. II.A). The objective of this work was to study the influence of light, electron radiation and temperature on the charging behavior of these solar panel components and to analyze the influence of adhesive and carbon mesh size. A numerical analysis has been carried out so as to understand the effect of the carbon mesh size on the charging potential of these elements. This paper aims then at demonstrating that satellite structures, supposedly highly conductive in space environment, may actually be submitted to hazardous charging potentials during an eclipse phase.

II. Experimental Setup and Protocol

A. Irradiation SIRENE Facility

The SIRENE experimental simulation facility reproduces the distributed electron spectrum in the range 5–400 keV and allows the assessment of charging potential and electric properties of space materials in geostationary (GEO) orbit conditions. The electron spectrum simulation is achieved by use of two monoenergetic electron beams (20 and 400 keV), these two beams being diffused in energy and angle to produce a spacelike electron flow with a good flux homogeneity, with flux variation lower than 15% in a 12 cm diameter area on the sample holder. Figure 1 shows the electron beam spectral characteristics of the SIRENE facility with an energy spectrum approaching that of the geostationary charging environment. The major interest of SIRENE is that it combines low energy

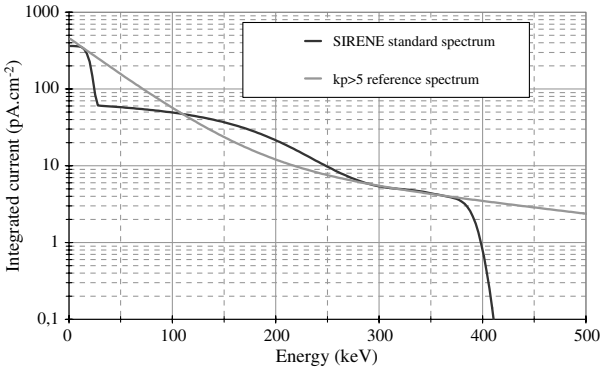

Fig. 1 The SIRENE electron beam spectral characteristics (integrated spectrum delivered by the complex diffusion window) and GEO $Kp > 5$ integrated reference spectrum.

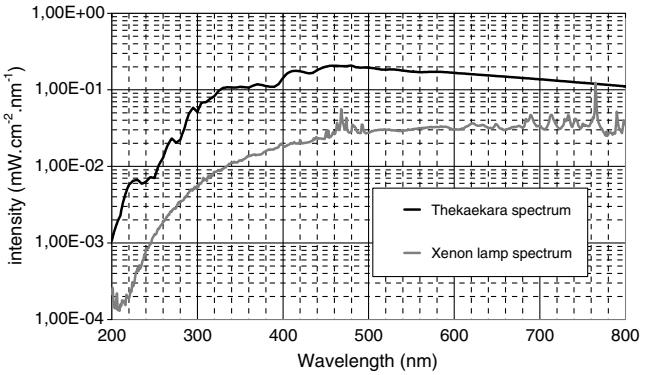

Fig. 2 Energy spectrum of the Xenon lamp installed in the SIRENE facility, compared with the Thekaekara standard solar spectrum.

electrons (that impinge and are implanted within the material bulk and induce electric charging) with higher energy electrons which go through the material without causing any charging but which contribute to modify its conductivity through the radiation induced conductivity mechanism. The nominal integrated fluxes used for the 20 keV monoenergetic beam and the distributed 0–400 keV one are, respectively, equal 250 and 50 pA.cm^{-2}. The temperature of the sample holder can be controlled in the range [−180°C, +150°C] allowing to reproduce the temperature variations of materials on flight. A pumping system allows experiments at vacuum of around 10^{-6} Torr.

A contactless electrostatic probe, combined with a *X-Y* motion system, scans the samples at around 5 to 8 mm from their surface and allows the evaluation of the surface potential of the materials. Surface potential is then continuously recorded during the experiments allowing the assessment of the electric conductivity as a function of time and electric field using the relation

$$\sigma(E) = \varepsilon_o \varepsilon \frac{\mathrm{d}V/\mathrm{d}t}{V} \tag{1}$$

This relation is derived from the electric potential relaxation after irradiation and by modelling the sample as a combination in parallel of a capacitance and resistance.

A Xenon lamp (Cunow, France) has been installed on the facility to simulate light radiation before and after the eclipse event. A quartz window has been installed on the facility to avoid any UV absorbance induced by the glass transmission. Figure 2 presents the energy spectrum delivered by the Xenon lamp, in comparison with the reference Thekaekara spectrum [5]. We can notice that the intensity level delivered by the Xenon lamp is 10 times lower than the standard spectrum. Despite this intensity difference, we have been able to notice a drastic effect of photon radiation on the electric charging of the samples.

B. Experimental Protocol

The experimental procedure was divided into four consecutive steps, simulating, respectively, the three consecutive flight situations: 1) before eclipse event at $Kp > 5$: electron irradiation of the samples at room temperature under light radiation (in a first preliminary stage, the sample have been submitted to 2 or 18 h photon radiation without electron radiation, in order to study the effect of residual photoconduction); 2) eclipse entry at $Kp > 5$: electron irradiation of the samples in darkness with decreasing temperature; and 3) eclipse exit at $Kp > 5$: electron irradiation of the samples under photon radiation with increasing temperature up to room temperature.

The electron radiation conditions similar to those encountered during a solar magnetic activity $Kp > 5$ are reproduced using the standard SIRENE spectrum produced with the following combined electron beam: (20 keV, 250 pA.cm^{-2}) (0–400 keV, 50 pA.cm^{-2}).

A former reference test has been performed following the same stages as described preceding but in darkness all along the different stages. It enables, in comparison with the following tests, to characterize the effect of photon radiation on the charging properties of solar panel structure and polyimide samples.

Tables 1–3 summarize the experimental protocol applied for the reference test and the "eclipselike" ones. We can notice in these tables that the temperature profiles are different from one test to the other. The specifications of the electrostatic probe implies to end phase 2 (eclipse phase) if the electric potential reaches around −8000 V at the surface of the samples. This limit potential is reached at different irradiation times (and therefore different operating temperatures) for the three different tests since light radiation history (and consequently the residual photoconduction level) differs from one test to the other. Phase 4 in each test is just a relaxation stage at room temperature and under light radiation to discharge the sample before the following test.

This experimental procedure allows the characterization of photoconduction and temperature effect on the electric potential of the polyimide surface.

III. Description of the Tested Samples

Three different samples have been tested in this study and basically differ from each other by the grounding path: one reference polyimide raw sample metallized on the rear face (to allow charge leakage) and two polyimide/adhesive samples. The two last samples

Table 1 Reference test (in darkness)

Test	Irradiation	Temperature	Light	Irradiation time
1.1	SIRENE spectrum	20°C	No	60 min
1.2	SIRENE spectrum	+20°C to −85°C	No	19 min
1.3	SIRENE spectrum	−85°C to +20°C	No	41 min
1.4	No irradiation	+20°C	Yes	120 min

Table 2 Eclipse test after 2 h light radiation: test 2

Test	Irradiation	Temperature	Light	Irradiation time
2.1	SIRENE spectrum	20°C	Yes	60 min
2.2	SIRENE spectrum	+20°C to −101°C	No	23 min
2.3	SIRENE spectrum	−101°C to +20°C	Yes	36 min
2.4	No irradiation	+20°C	Yes	120 min

Table 3 Eclipse test after 18 h light radiation: test 3

Test	Irradiation	Temperature	Light	Irradiation time
3.1	SIRENE spectrum	20°C	Yes	60 min
3.2	SIRENE spectrum	+20°C to −137°C	No	26 min
3.3	SIRENE spectrum	−137°C to +20°C	Yes	27 min
3.4	No irradiation	+20°C	Yes	120 min

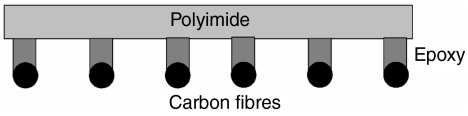

Fig. 3 Sketch of the polyimide/adhesive samples.

are stacking of 50 μm thick polyimide film, 50 μm thick epoxy resin (see Fig. 3) and a conductive carbon mesh and vary only by the carbon mesh size, as seen in Fig. 4. For the polyimide/adhesive samples, the connection to the ground is performed through the carbon fibers electric contact. The path length of the implanted electron between the irradiated surface and the ground differs from one sample to the other. This choice enables to study the effect of adhesive and mesh size on the overall charging potential of the system during the different experimental stages.

IV. Experimental Results

A. Reference Test

This first test is a reference test performed in darkness. It aims to discriminate, in comparison with the following tests, the effect of light radiation from the effect of temperature on the charging potential built up at the surface of the samples.

1. *Phase 1.1: Before the Eclipse Phase*

Figure 5 presents the evolution of the charging potential built up on the three samples during the reference test. We can notice drastic differences between the reference polyimide sample and the two polyimide/adhesive ones. During phase 1, the reference sample reaches an electric potential equal to around −800 V, in comparison with a potential close to −6400 V and −6500 V for the other high-density and low-density samples. The low-density sample presents as well a charging kinetics at the start of the test much higher than the high-density one. The path length of the electron between the surface and the ground being higher for the low-density sample, the equivalent dielectric capacity of this latter is then reduced in comparison with the high-density sample and the reference one, leading then to a significant increase of the charging kinetics. The huge increase of equilibrium potential for the polyimide/adhesive samples, in comparison with the reference one, is directly assigned to a large rise of the equivalent electric resistance due to the sample design: the adhesives enlarge the resistive path of the electrons to the ground and the lack of metallization on the rear face of the polyimide film adds a surface resistive element on this face. Figure 6 summarizes the electron path from the surface to the ground. This steep increase in the absolute charging potential between the reference sample and the polyimide/adhesive samples can be ascribed as well to the high energy electrons which go through the polyimide film and are implanted directly within the adhesive films. A higher quantity of incident electrons take part to the charging process in the polyimide/adhesive samples, leading then a higher absolute charging potential. At this stage, we cannot notice any strong influence of the fiber mesh since the equilibrium potential is

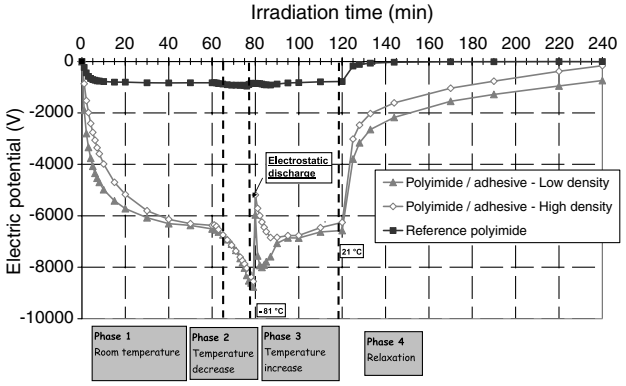

Fig. 5 Evolution of the electric charging level built up on the three tested samples during the different phases of the reference test (in darkness).

quite similar for both polyimide/adhesive samples. The selection of adhesive can significantly determine the charging potential of these samples, which have already reached hazardous charging level after 60 min irradiation in darkness at room temperature.

2. *Phase 1.2: Eclipse Entry*

During the second phase, the samples are irradiated in darkness with a decreasing applied temperature. The reference sample does not present any potential drop when temperature decreases, in opposition with the polyimide/adhesive samples, the absolute charging level of which rising swiftly with the decreasing temperature. We have already demonstrated [6] that adhesives are highly sensitive to temperature, their electric conductivity falling down quickly with the applied temperature. The same feature is observed in the current situation with a charging potential mainly ruled by the epoxy adhesive system. This phase had to be stopped after 19 min due to the very high hazardous potential (−9000 V) measured on both polyimide/adhesive samples.

3. *Phase 1.3: Eclipse Exit*

During phase 3, the samples are still irradiated with an increasing temperature (up to room temperature). We can notice, at the start of this phase, a steep decrease of the absolute charging potential which is a feature of an electrostatic discharge, likely to occur between the surface of the samples and the electrostatic probe. This electrostatic discharge is initiated by the high electric potential built up at the surface of the samples. It must take place between the surface of the sample and the electrostatic probe (the potential of which varying when the probe sweeps from the ground to the sample).

After a transitory phase following this discharge, we can notice that the absolute charging potential of both polyimide/adhesive samples drops down continuously to reach, at room temperature, the same equilibrium potential met before the eclipse entry. Temperature is therefore the main parameter steering the charging potential of the

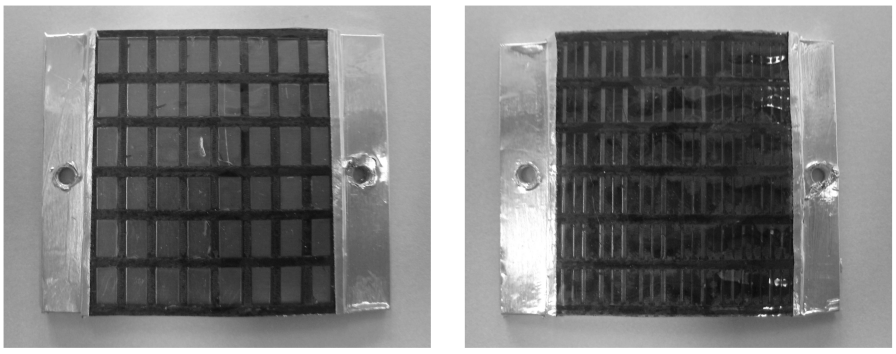

a) **b)**

Fig. 4 View of the two polyimide/adhesive samples: a) low-density carbon fibers mesh and b) high-density carbon fibers mesh.

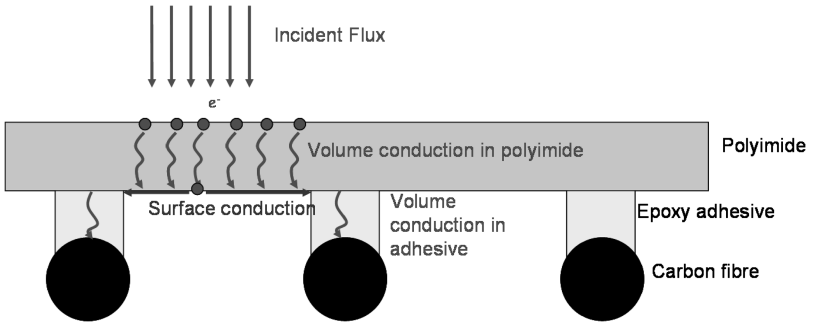

Fig. 6 Sketch presenting the electron path in the polyimide/adhesive samples from its surface to the ground.

polyimide/adhesive samples. In so far as we do not observe any variation of the charging potential on the reference sample, we can easily conclude that temperature mainly affect the adhesive conductivity: as temperature decreases, this electric conductivity drops down dramatically.

The last phase (phase 4) of this reference test aims only to discharge the sample under light radiation before the following eclipse test.

B. Test 2: Eclipse Simulation Following Two-Hour Light Radiation

This second test aims to simulate an eclipse event before 2 h light radiation without any incident electron flux. Comparing with test 3 (for which we applied 18 h light radiation before the eclipse simulation), we will be able to study the effect of photoconductivity on the charging potentials.

1. Phase 2.1: Before the Eclipse Phase

During this phase, the samples are irradiated using the standard SIRENE electron spectrum, under light radiation at room temperature. We simulate the situation before the eclipse phase during a high solar magnetic period. Figure 7 presents the evolution of the charging potential built up on the three samples during this second test. We can notice that the reference polyimide sample reaches an equilibrium potential equal to −300 V, which is noticeably lower that the one measured during the reference test, thanks to the photon induced conductivity. The charging potential reached by the polyimide/adhesive samples is equal to −2700 V for the high-density sample and −3600 V for the low-density sample. In comparison with the reference test results, we can first notice an important decrease of the absolute charging potential on both samples with light radiation: the upper polyimide film is submitted to an intense photon induced conductivity allowing dragging the electrons to the ground in a more efficient way, leading then to a lower absolute potential. The second observation is the buildup of a potential difference between the two polyimide/adhesive samples, which demonstrates the influence of fiber mesh size on charging level. A physical model coupled with numerical analysis has been performed to understand this evolution and difference between both polyimide/adhesive samples and identify the main physical mechanisms accounting for this difference. This numerical analysis will be presented in the last section of this paper.

A first physical explanation is described hereafter. As pictured in Fig. 6, the low energy (0–20 keV) electrons are first implanted at the surface of the sample. They can then drift within the polyimide volume under the effect of the applied electric field and the electric conductivity enhanced by photon and high energy electron radiation. Once they reach the rear face of the polyimide film, the only way to be dragged to the ground is to flow along the rear surface thanks to the surface conductivity likely as well to be enhanced by photon and high energy electrons. Once they reach the epoxy adhesive location, they can then easily flow away to the ground through the thin adhesive film. For the same increase of the volume conductivity of polyimide under photon and electron radiation, the total volume resistance decrease in a square element (as described in Fig. 8) within the polyimide film should be higher for the high fiber density samples (this resistance is in inverse proportion to the square of the fiber distance). As a consequence, when the samples are submitted to light radiation, the absolute potential decrease (in comparison with the reference test) will be higher for the high fiber density, as observed during test 2. The effect of fiber mesh size will be described in more details in the last sections describing the numerical analysis.

2. Phase 2.2: Eclipse Entry

As for the reference test, the samples are irradiated in darkness with a decreasing applied temperature during the second phase. We can notice an interesting feature on the reference polyimide. During this second phase, the charging potential of this sample decreases continuously with time. The sample is not radiated with light: the effect of this light radiation sustains a residual photon induced conduction which falls down gradually leading to a continuous increase of the absolute charging potential (due to the enhancement of the total resistance of the system). This feature was not observed during the reference test since no photoconduction was initiated within the sample. The charging potential of the reference sample during this second test gets then close to the one measured during the reference test at the end of the eclipse entry: we can then assume that

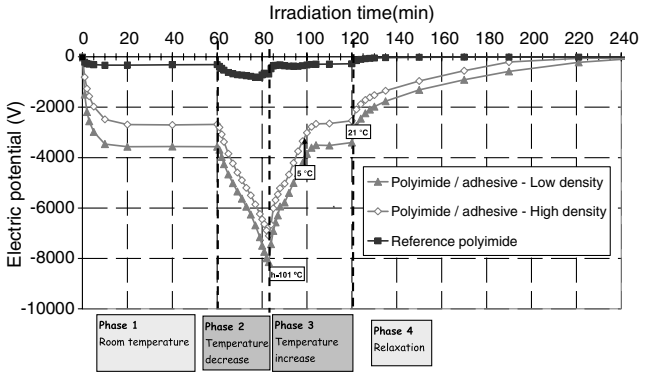

Fig. 7 Evolution of the electric charging level built up on the three tested samples during the different phase of test 2.

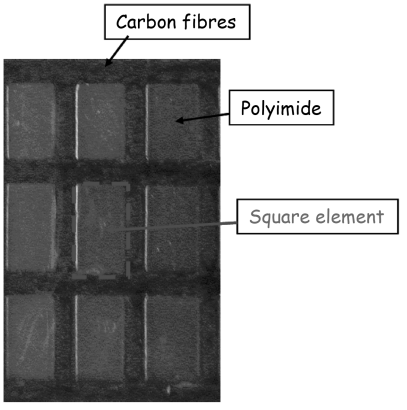

Fig. 8 Description of a square polyimide element.

photoconduction has lowered dramatically and that its effect on charging potential is insignificant. At this stage of the study, we do not know if this photoconduction drop is ascribed to low temperature effect or to a temporal relaxation of this mechanism, since both temperature drop and light shutdown occur at the same time.

The behavior of the polyimide/adhesive samples is quite similar to the one observed in the reference test. The potential difference between both samples is still maintained during the eclipse exit and the absolute charging potentials in this test are lower than those observed in the reference test at the same temperature level. However, the potential difference is lower than the difference measured at room temperature before the eclipse phase: we measure a potential difference between both tests equal to −1000 V at 85°C for the low-density sample, to be compared with −2600 V at room temperature. We can indeed notice that the potential drop kinetics is higher during this test (around -190 V.min^{-1} vs -120 V.min^{-1} for the reference test) for the same temperature kinetics. This higher potential decrease can still be ascribed to the relaxation of photoconduction, either with time or temperature. Light radiation effect is therefore quickly annealed during the eclipse phase leading to hazardous potentials after 20 min irradiation and −100°C. For the potential probe safety, the eclipse phase had to be stopped at this temperature level.

3. Phase 2.3: Eclipse Exit

The behavior of the polyimide/adhesive samples during the eclipse exit is similar to the one observed in the reference test. Once the samples are heated up, their absolute charging potential decreases due to an increase of the adhesive electric conductivity. These samples recover the charging potential measured before the eclipse entry, for a temperature equal to around 5°C. The effect of temperature is therefore effective for temperature lower than 5 °C but can be considered as insignificant above this level. For temperatures higher than 5°C, the charging potential is basically steered by photon induced conductivity (instantaneous during light radiation, or residual in darkness). At the start of the eclipse exit and for the three samples, we can observe a dramatic decrease of the absolute charging potential: this emphasizes the effect of the instantaneous photoconduction (or photoemission) which rapidly drags away the electrons implanted in the volume during the eclipse phase.

C. Test 3: Eclipse Simulation Following 18 Hour Light Radiation

This third test aims to simulate an eclipse event before 18 h light radiation without any incident electron flux.

1. Phase 3.1: Before the Eclipse Phase

During this phase, the samples are irradiated using the standard SIRENE electron spectrum, under light radiation at room temperature. Figure 9 presents the evolution of the charging potential built up on the three samples during this third test. The reference polyimide sample reaches a charging potential equal to −210 V which is 100 V higher than the one measured in test 2. This feature

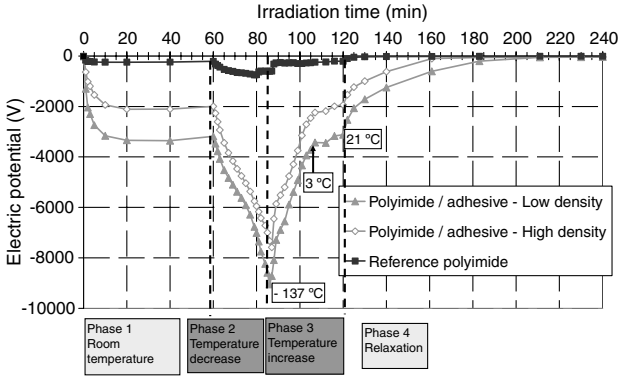

Fig. 9 Evolution of the electric charging level built up on the three tested samples during the different phase of test 3.

should be explained by an increase of the total dose transmitted to the material under light radiation (before the electron radiation) which led to a higher residual photoconductivity during phase 1 and consequently a lower absolute charging potential. The two polyimide / adhesive samples reach charging potentials equal, respectively, to −2000 V for the high-density sample (to be compared with −2700 V measured in test 2) and −3200 V for the low-density sample (to be compared with −3600 V measured in test 2). This overall absolute decrease is ascribed, as explained earlier, to a higher residual photoconductivity induced by a longer light preradiation. We can notice as well an increase of the charging potential difference between both polyimide/adhesive samples: this differences rises from 900 V for 2 h light radiation to 1200 V for 18 h light radiation.

2. Phase 3.2: Eclipse Entry

As observed in test 2, we can notice that the charging potential of the reference sample drops down with the temperature. This can be assigned to the decrease of photoconductivity due either to the low temperature effect or to a temporal relaxation. The behavior of the polyimide/adhesive samples keeps up the same feature as observed in test 2, with a dramatic decrease of the charging potential with temperature. We can as well notice that the charging potential difference (in comparison with the reference test) gradually fades away: we measure a potential difference between both tests (test 3 and the reference test) equal to −1300 V at −85°C for the low-density sample, to be compared with −3300 V at room temperature. However, the potential drop kinetics measured on the polyimide/adhesive samples is quite similar to those measured in test 2 (-180 V.min^{-1} for test 3 vs -190 V.min^{-1} for test 2). This feature suggests then that the residual photoconduction relaxes rapidly in both tests, despite a total initial radiation dose higher in the second test. During the eclipse event, the charging potential of these samples is then basically ruled by the sole effect of temperature. For safety reason, the eclipse phase had to be stopped at −137°C (and a potential level of −9000 V).

3. Phase 3.3: Eclipse Exit

As observed in test 2, the charging potential of the three samples increases swiftly at the start of the eclipse exit under the effect of the instantaneous photoconduction. The polyimide/adhesive samples recover the equilibrium potential measured before the eclipse phase, at a temperature equal to 3°C, which is approximately the same as the temperature threshold assessed in test 2. These experimental characteristics confirm the first conclusions stated in test 2: temperature effect prevails over photoconduction for thermal level lower than this threshold. Above 3°C, photoconduction should be the major parameter steering the charging potential of the polyimide/adhesive samples.

V. Numerical Analysis

A. Physics Model

During the different experimental tests, we have noticed strong variations in the electric features of the two polyimide/adhesive samples. For each test, the low-density sample presents always a higher absolute electric potential in comparison with the other one. The charging potential difference is enhanced through light illumination. Moreover, the absolute charging potential of both samples is around two to three times higher than the charging potential of a conventional reference polyimide sample tested in the same conditions. These differences are therefore directly linked to the presence of fibers and adhesives on the real samples. A physical model has been devised in this study so as to account for the evolution of the charging potential of the real samples during the first stage of the experiments (before the eclipse phase). This model is described hereafter.

Each sample can actually be defined as a network of several square elements presenting the same charging potential. At first stage, we can indeed assume that the electrons implanted in the polyimide film may diffuse to the film rear face rather than on the surface since the

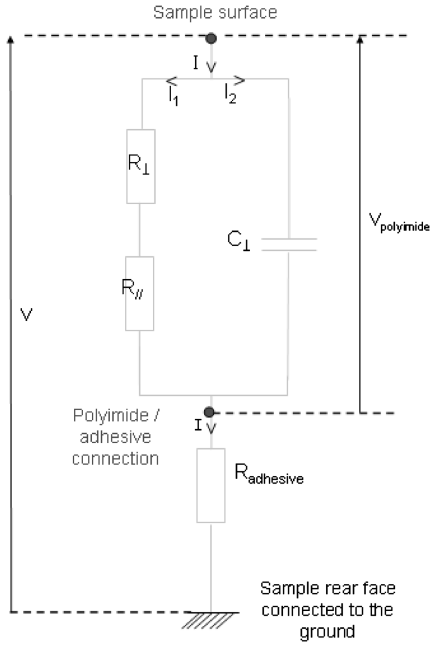

Fig. 10 Equivalent electric diagram of the polyimide/adhesive system (symbols ⊥ and // are related to the volume and surface resistance and capacitance).

surface electric field must be much weaker than the electric field created in the bulk. We can then take as unique element a sole square element for our numeric calculation. This element is a system composed of polyimide film, epoxy adhesive and carbon fibers. For this element, we can assume that the incident electrons diffuse at first step in the volume of the polyimide film. Once they have reached the polyimide film rear face, they can diffuse at the surface of the film to reach the adhesive location. They can then diffuse within the adhesive film and reach the carbon fibers connected to the ground. This process is described in Fig. 6. We assume in our calculation that the element is a perfect square. For both real samples, the interfiber distance is then equal to 1.6 mm for the high-density fiber sample and 3.2 mm for the low-density fiber sample. The equivalent electric diagram can then be written as described in Fig. 10 (the carbon fiber are supposed to be highly conductive).

For the assessment of the charging potential reached by the sample, we need first to consider the charging behavior of a discrete element which width is dx (Fig. 11). In an equilibrium stage (constant charging potential), the dielectric capacitance does not charge anymore (the electric current gets constant and is an equilibrium between the incident current and the conduction current). The equilibrium charging potential can then be written as

$$V_{\text{lim}} = (R_{\perp} + R_{//} + R_{\text{ad}}).I \tag{2}$$

where V_{lim} is the equilibrium potential reached on the discrete element, $R_{\perp}$ the volume resistance, $R_{//}$ the surface resistance for the abscise x, R_{ad} the adhesive resistance and I the incident electric current.

We can write for each parameters with the following equations:

$$I = J.d_{\text{fibre}}.\text{d}x \tag{3}$$

$$R_{//}(x) = \frac{x}{d_{\text{fibre}}} R_{sq} \tag{4}$$

$$R_{\perp}(x) = \rho_{\perp} . \frac{e_{\perp}}{d_{\text{fibre}}.\text{d}x} \tag{5}$$

$$R_{\text{ad}} = \rho_{\text{ad}} . \frac{e_{\text{ad}}}{d_{\text{fibre}}.d_{\text{ad}}} \tag{6}$$

where J is the incident electron current per surface area, d_{fibre} the interfiber distance, $R_{//}$ the surface resistance related to the discrete element irradiated at location x, R_{sq} the sheet resistance, x the distance between the carbon fiber and the related discrete element, $R_{\perp}$ the volume resistance related to the discrete element in the polyimide film, $\rho_{\perp}$ the volume resistivity of polyimide, $e_{\perp}$ the polyimide film thickness, R_{ad} the volume resistance of the adhesive film at location $x = 0$, ρ_{ad} the adhesive volume resistivity, e_{ad} the adhesive thickness and d_{ad} the adhesive width at location $x = 0$.

The charging potential reached on the discrete element can then be written as

$$V_{\text{lim}}(x) = \left(\frac{x}{d_{\text{fibre}}} R_{sq} + \rho_{\perp} \frac{e_{\perp}}{d_{\text{fibre}}.dx} + \rho_{\text{ad}} \frac{e_{\text{ad}}}{d_{\text{fibre}}.d_{\text{ad}}} \right) .J.d_{\text{fibre}}.\text{d}x \tag{7}$$

$$V_{\text{lim}}(x) = x.R_{sq}.J.\text{d}x + \rho_{\perp}.e_{\perp}.J + \rho_{\text{ad}} \frac{e_{\text{ad}}}{d_{\text{ad}}} .J.\text{d}x \tag{8}$$

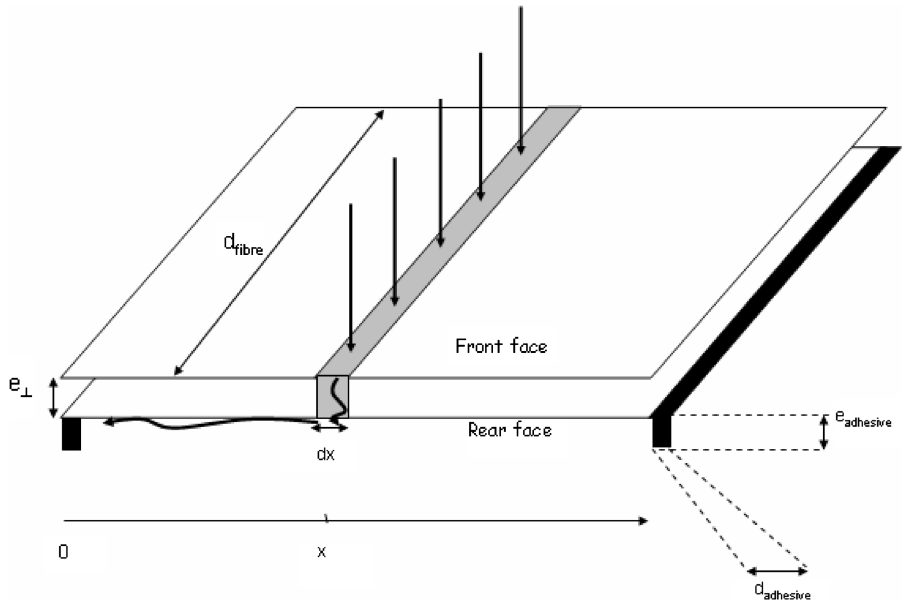

Fig. 11 Presentation of a discrete element for the evaluation of the charging potential of the polyimide/adhesive samples.

The total charging potential at the center of the square element is the sum of the charging potential differences initiated in all discrete elements. We need then to integrate the previous relation to get this central theoretical potential:

$$V_{\lim} = \rho_{\perp}.e_{\perp}.J + \int_{x=0}^{d_{\text{fibre}}} (x.R_{sq}.J.\mathrm{d}x) + \int_{x=0}^{d_{\text{fibre}}} \left(\rho_{\text{ad}} \frac{e_{\text{ad}}}{d_{\text{ad}}}.J.\mathrm{d}x\right) \quad (9)$$

$$V_{\lim} = \rho_{\perp}.e_{\perp}.J + \frac{R_{sq}}{2}.d_{\text{fibre}}^2.J + \rho_{\text{ad}} \frac{e_{\text{ad}}}{d_{\text{ad}}}.d_{\text{fibre}}.J \quad (10)$$

From Eq. (10), we can get the different equilibrium potentials reached by the high-density (H) and low-density (L) fibers samples:

$$V_{\lim H} = \rho_{\perp}.e_{\perp}.J + \frac{R_{sq}}{2}.d_{\text{fibre}H}^2.J + \rho_{\text{ad}} \frac{e_{\text{ad}}}{d_{\text{ad}}}.d_{\text{fibre}H}.J \quad (11)$$

$$V_{\lim L} = \rho_{\perp}.e_{\perp}.J + \frac{R_{sq}}{2}.d_{\text{fibre}L}^2.J + \rho_{\text{ad}} \frac{e_{\text{ad}}}{d_{\text{ad}}}.d_{\text{fibre}L}.J \quad (12)$$

The sheet resistance and the adhesive volume resistivity can then be derived from Eqs. (11) and (12):

$$R_{sq} = \frac{2}{d_{\text{fibre}H} - d_{\text{fibre}F}}.\left[\frac{1}{J}\left(\frac{V_{\lim H}}{d_{\text{fibre}H}} - \frac{V_{\lim F}}{d_{\text{fibre}F}}\right) - \rho_{\perp}.e_{\perp}.\left(\frac{1}{d_{\text{fibre}H}} - \frac{1}{d_{\text{fibre}F}}\right)\right] \quad (13)$$

$$\rho_{\text{ad}} = [V_{\lim H} - \rho_{\perp}.e_{\perp}.J - \frac{R_{sq}}{2}.d_{\text{fibre}H}^2.J]\frac{d_{\text{ad}}}{e_{\text{ad}}}.\frac{1}{d_{\text{fibre}H}.J} \quad (14)$$

From this numerical model and the previous equations, the unknown parameters are the following: R_{sq}, ρ_{ad} and $\rho_{\perp}$. The other model parameters are given in Table 4.

In this model, we assume that the charging potential of the samples is mainly ruled by the low energy (20 keV) electrons the current density of which being equal to 250 pA.cm^{-2}. However, the high energy electrons would contribute to the increase of the volume electric conductivity of the polyimide film (radiation induced conductivity). During the charging process, the sample gets negatively charged and the incident electrons are consequently slowed down, inducing then a continuous decrease of the current density. The evolution of the current density J is given by the following relation:

$$J = e.n_e.v = e.n_e.\sqrt{\frac{2.\xi(t)}{m_e}} = e.n_e.\sqrt{\frac{2.[\xi_0 - eV(t)]}{m_e}} \quad (15)$$

where e is the electron charge ($e = 1,6\,10^{-19}$ C), ξ_0 the initial incident energy (equal to 20 keV), $\xi(t)$ the electron energy as a function of time, $V(t)$ the surface charging potential, m_e the electron mass ($=9,1.10^{-31}$ kg), v the electron velocity and n_e the electron density which can be assessed from the initial current density and the initial incident energy ξ.

Adjusting the model parameters implies to fit the experimental evolution $V(t)$ during the first phase (before the eclipse), with the theoretical potential evolution which can be expressed by the following relation:

Table 4 Physical parameters used in the model

Parameters	Values
$e\perp$	50.10^{-6} m
$d_{\text{fibre}H}$	$1.6\,10^{-3}$ m
$d_{\text{fibre}F}$	$3.2\,10^{-3}$ m
d_{ad}	10^{-3} m
e_{ad}	50.10^{-6} m

$$\frac{\mathrm{d}V}{\mathrm{d}t} + \frac{V}{(R_{\perp} + R_{//}).C_{\perp}} = \frac{(R_{\perp} + R_{//} + R_{\text{ad}}).I}{(R_{\perp} + R_{//}).C_{\perp}} + R_{\text{ad}}.\frac{\mathrm{d}I}{\mathrm{d}t} \quad (16)$$

To a first approximation, we can state that the parameter $\frac{\mathrm{d}I}{\mathrm{d}t}$ is very low, leading then to the following relations:

$$\frac{\mathrm{d}V}{\mathrm{d}t} + \frac{V}{(R_{\perp} + R_{//}).C_{\perp}} = \frac{(R_{\perp} + R_{//} + R_{\text{ad}}).I}{(R_{\perp} + R_{//}).C_{\perp}} \quad (17)$$

$$V(t) = (R_{\perp} + R_{//} + R_{\text{ad}}).I(t).\left[1 - \exp\left(-\frac{t}{(R_{\perp} + R_{//}).C_{\perp}}\right)\right] \quad (18)$$

B. Analytical Method for Parameters Extraction

The physics model should enable to understand more clearly the evolution of the charging potential of the different samples and especially to analyze the effect of light irradiation on the increase of charging potential difference observed between both real samples at room temperature.

The basic equations allowing a study on the charging potential evolution and the extraction of the model parameters are summarized hereafter:

$$R_{sq} = \frac{2}{d_{\text{fibre}H} - d_{\text{fibre}L}}.\left[\frac{1}{J_{\lim}}\left(\frac{V_{\lim H}}{d_{\text{fibre}H}} - \frac{V_{\lim L}}{d_{\text{fibre}L}}\right) - \rho_{\perp}.e_{\perp}.\left(\frac{1}{d_{\text{fibre}H}} - \frac{1}{d_{\text{fibre}L}}\right)\right] \quad (19)$$

$$\rho_{\text{ad}} = \left[V_{\lim H} - \rho_{\perp}.e_{\perp}.J_{\lim} - \frac{R_{sq}}{2}.d_{\text{fibre}H}^2.J_{\lim}\right]\frac{d_{\text{ad}}}{e_{\text{ad}}}.\frac{1}{d_{\text{fibre}H}.J_{\lim}} \quad (20)$$

$$V(t) = (R_{\perp} + R_{//} + R_{\text{ad}}).I(t).\left[1 - \exp\left(-\frac{t}{(R_{\perp} + R_{//}).C_{\perp}}\right)\right] \quad (21)$$

$$I(t) = d_{\text{fibre}}^2.J(t) \quad (22)$$

$$J(t) = e.n_e.\sqrt{\frac{2.[\xi_0 - eV(t)]}{m_e}} \quad (23)$$

where $J_{\lim}$ is the current density during the equilibrium stage.

Four unknown parameters must be extracted from the experimental data: the sheet resistance at the rear face of the polyimide film R_{sq}, the volume resistivity of the polyimide film $\rho_{\perp}$, the volume resistivity of adhesive ρ_{ad}, and the dielectric capacitance of the polyimide films $C_{\perp}$. The analytic method used for the extraction of these different parameters is divided into several consecutive steps: 1) operator-provided initial value for $\rho_{\perp}$ (based on data tables provided by the supplier or previous measurements); 2) evaluation of R_{sq} and ρ_{ad} from Eqs. (19) and (20) and using the initial value for the current density (250 pA.cm^{-2}); 3) evaluation of $C_{\perp}$ from the assessed values of $\rho\perp$, R_{sq} and ρ_{ad}, using the following relation:

$$C_{\perp} = \frac{(R_{\perp} + R_{//} + R_{\text{ad}}).I(0)}{(R_{\perp} + R_{//}).(\frac{\mathrm{d}V}{\mathrm{d}t})_{t=0}} \quad (24)$$

and $J(0) = 250$ pA.cm^{-2}; 4) evaluation of $V(t)$ using the following relation: a) $J(0) = 250$ pA.cm^{-2}, b) $V(t) = (R_{\perp} + R_{//} + R_{\text{ad}}).I(t).\left[1 - \exp\left(-\frac{t}{(R_{\perp}+R_{//}).C_{\perp}}\right)\right]$, c) $J(t + \Delta t) = e.n_e.\sqrt{\frac{2.[\xi_0 - eV(t)]}{m_e}}$, and d) evaluation of $V(t + \Delta t)$; 5) evaluation of $J_{\lim}$; 6) new evaluation of R_{sq}, ρ_{ad} and $C_{\perp}$; and 7) evaluation of $V(t)$ and iteration on $\rho_{\perp}$, $J_{\lim}$, R_{sq}, ρ_{ad} and $C_{\perp}$ for a good fit with the experimental data.

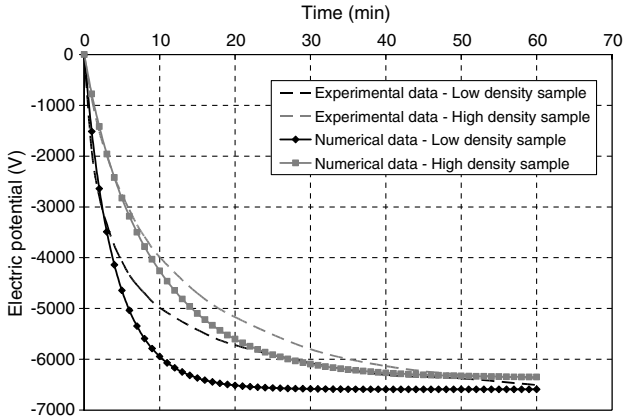

Fig. 12 Evolution of the charging potential assessed experimentally and numerically for both low and high-density polyimide/adhesive samples during phase 1 of test 1.

This extraction method has been applied on phase 1 for the three tests: it should then be possible to understand which parameter is the most sensitive to light radiation and get a clearer view on the effect of mesh size on the charging potential of the polyimide/adhesive samples.

C. Numerical Results

The numerical results, coupled with a comparison with the experimental data, are presented for the three tests in Figs. 12 (test in darkness), 13 (test after 2 h light radiation) and 14 (test after 18 h light radiation). We can notice a fairly good fit between the experimental and numerical data for tests 2 and 3. Some differences can be observed in test 1 between the experimental and numerical graphs. These can be explained to the fact that equilibrium on charging potential is not reached after 60 min irradiation, leading to possible significant errors in the assessment of the equilibrium charging potential. These errors could lead to important inaccuracies in the estimation of the different model parameters $\rho_{\perp}$, R_{sq} and ρ_{ad}. For tests 2 and 3, the charging potential equilibrium is reached leading then to a better precision for the assessed model parameters. From this numerical graphs, we can, however, notice that the current physics model allows accounting for the quantitative and qualitative features observed experimentally. We can especially observe numerically that the potential difference between both samples is enhanced with the increase of light irradiation. This difference is evaluated numerically at 240 V for test 1, 830 V for test 2 and 1170 V for test 3, vs 230, 890 and 1230 V measured experimentally.

Figures 15–17 present the evolution of the sheet resistance, the polyimide volume resistivity and the adhesive volume resistivity as a function of light radiation time performed before the tests. We can notice from these figures that the polyimide surface resistivity as well as the adhesive volume resistivity are not strongly affected by light radiation. This is basically due to the fact that depth penetration of UV radiation (which is responsible of photoconductivity process) is very low in comparison with the polyimide film thickness. As a conclusion of this process, the polyimide rear face and the adhesive film are not submitted to noticeable UV radiation which leads then to

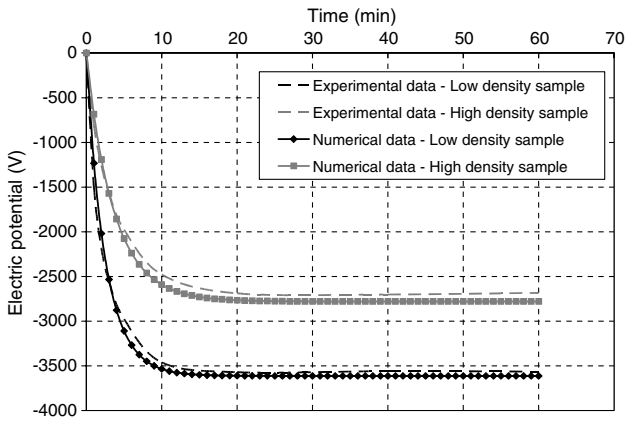

Fig. 13 Evolution of the charging potential assessed experimentally and numerically for both low- and high-density polyimide/adhesive samples during phase 1 of test 2.

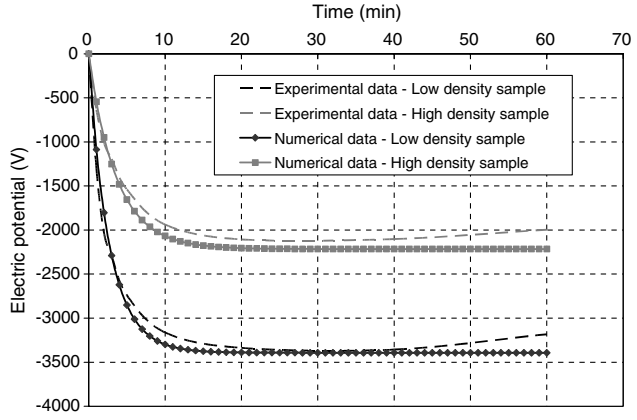

Fig. 14 Evolution of the charging potential assessed experimentally and numerically for both low- and high-density polyimide/adhesive samples during phase 1 of test 3.

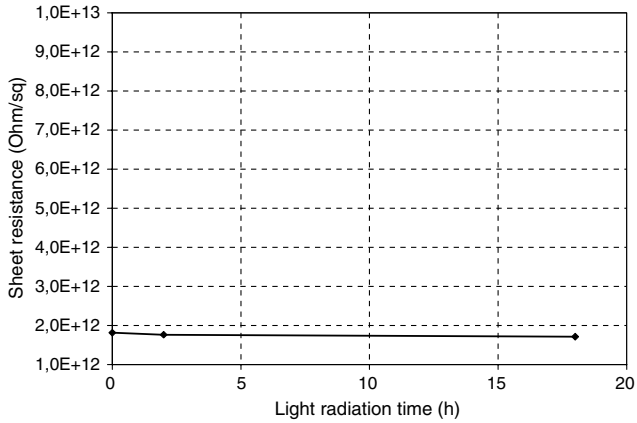

Fig. 15 Evolution of sheet resistance at the rear face of the polyimide film for both polyimide/adhesive samples as a function of light radiation time performed before the tests.

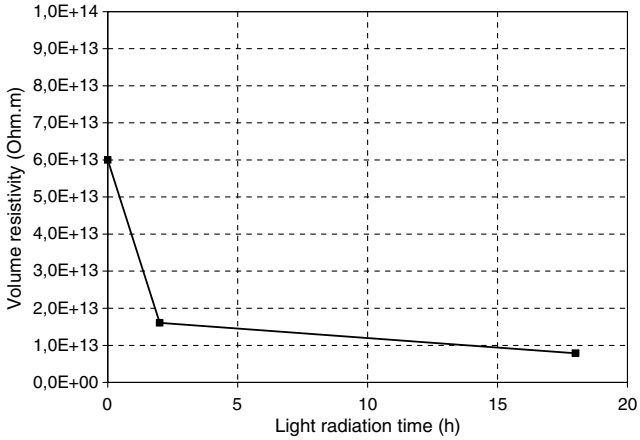

Fig. 16 Evolution of the volume resistivity of the polyimide film for both polyimide/adhesive samples as a function of light radiation time performed before the tests.

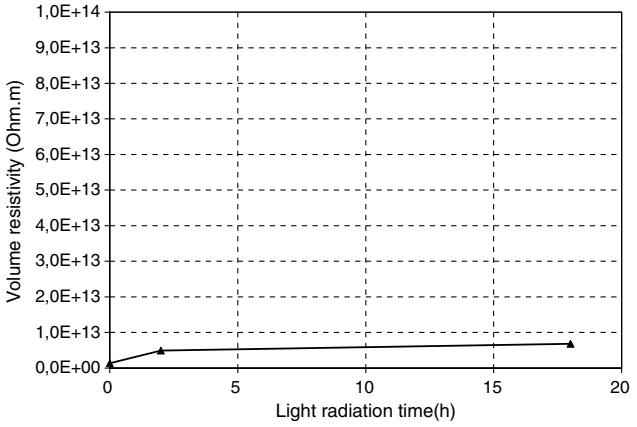

Fig. 17 Evolution of the volume resistivity of the adhesive film for both polyimide/adhesive samples as a function of light radiation time performed before the tests.

a weak variation of both parameters. We can notice slight variation of the adhesive volume resistivity which might be ascribed to model and measurements inaccuracies.

As stated in the previous section describing the experimental data, the numerical results show that light radiation induces a dramatic decrease of polyimide volume resistivity, thanks to the photoconductivity mechanism. The evolution of charging potential and the increase of the potential difference between both samples with light radiation are therefore mainly steered by the volume conductivity of the polyimide film. The volume resistance of a polyimide square element (expressed, to a first approximation, by the relation $R_{\perp} = \rho_{\perp} \frac{e_{\perp}}{d^2_{\text{fibre}}}$) drops down more rapidly when the surface area of the square element is small since the resistivity variation is expressed by the relation $\Delta R_{\perp} = \Delta\rho_{\perp} \frac{e_{\perp}}{d^2_{\text{fibre}}}$. The density of the carbon fiber mesh steers therefore at great level the charging potential of these samples by affecting significantly the volume resistance of the adjacent polyimide cells (or square elements).

Looking quantitatively at the numerical data, we can notice a polyimide volume resistivity close to 5.10^{13} Ω.m. The supplier data provided for this 200HN polyimide is $1.5\,10^{15}$ Ω.m, which is 2 decades higher than the assessed value. This difference can be assigned to the effect of the high energy electrons which transfer a significant radiation dose in the polyimide bulk leading then to an noticeable enhancement of the volume conductivity (radiation induced conductivity). For the same reason, the elevated value assessed for the sheet resistance (around 10^{12} Ω/sq) put forward a high radiation induced conductivity initiated at the rear face of the polyimide film by the high energy electrons (above 80 keV) which are able to go through this film and inject a high quantity of radiation dose (the common values given by the supplier are close to 10^{16} Ω/sq). A total electron flux of around 30 pA.cm^{-2} can reach the rear face of the polyimide film, leading then to a radiative dose rate equal to around 0.25 Gy.s^{-1} and a total radiative dose after 60 min irradiation equal to 860 Gy. As demonstrated in reference [2] this radiative dose rate is sufficient to trigger a conspicuous induced conductivity within or at the surface of the polyimide film.

VI. Conclusions

The current work aimed to study the charging behavior of polyimide/adhesive systems used on solar panels, during an eclipse event. The experimental protocol devised for this study allowed the analysis of the effect of temperature and photoconduction (instantaneous or residual) on the charging potential of these samples. From this study, it can be concluded that epoxy adhesives determine at a great level the system charging potential, especially at low temperature. It has indeed been demonstrated that the electric conductivity of these adhesives dramatically drops down with temperature leading to hazardous surface charging potential. Moreover, light radiation induces significant photon induced conductivity within the polyimide films allowing the reduction of the absolute charging level. However, this effect gets rapidly insignificant during the eclipse phase. This feature has been assigned to the dramatic relaxation of residual photoconductivity, leading then to hazardous charging levels despite a light preradiation. It has also been possible to put in evidence the huge effect of carbon fiber mesh size on the charging level: a denser fiber mesh enables to reduce significantly the electric potential outside the eclipse phase. Dramatic differences can be observed between two samples presenting a different fiber density. A high-density of carbon fibers enables to reduce significantly the absolute charging potential reached at the surface of the system. The numerical analysis described in this paper enabled to demonstrate that light radiation especially affect the volume resistivity of the polyimide film. Sheet resistance and the adhesive volume resistivity seem to keep up the same value for the first phase of the different test (before the eclipse phase). The enhancement of the potential difference between both samples has therefore been assigned to the increase of polyimide volume conductivity with light radiation.

Acknowledgment

The authors would like to thank Centre National d'Etudes Spatiales Research and Technology for having prepared the financial, technical, and scientific environment of these experiments.

References

[1] Levy, L., Paulmier, T., Dirassen, B., Inguimbert, C., and Van Eesbeek, M., "Aging and Prompt Effects on Space Material Properties," *IEEE Transactions on Plasma Science*, Vol. 36, No. 5, 2008, pp. 2228–2237. doi:10.1109/TPS.2008.2002914

[2] Paulmier, T., Dirassen, B., Payan, D., and Van Eesbeek, M., "Material Charging in Space Environment: Experimental: Test Simulation and Induced Conductive Mechanisms," *IEEE Transactions on Dielectrics and Electrical Insulation*, Vol. 16, No. 3, June 2009, pp. 682–688.

[3] Weingart, R. C., Barlett, R. H., Lee, R. S., and Hofer, W., "X-Ray-Induced Photoconductivity in Dielectric Films," *IEEE Transactions on Nuclear Science*, Vol. 19, No. 6, 1972, pp. 15–22. doi:10.1109/TNS.1972.4326804

[4] Kan, L., and Kao, K. C., "Photoconduction in Polyimide," *Conference Record of the 1990 IEEE International Symposium on Electrical Insulation*, 3–6 June 1990, pp. 84–87.

[5] Thekaekara, M. P., ed., *The Solar Constant and the Solar Spectrum Measured from a Research Aircraft*, NASA, Washington, D.C., 1970.

[6] Paulmier, T., Dirassen, B., Payan, D., and Balcon, N., "Charging Behavior of Space used Adhesives at Low Temperature in Geostationary Orbit," *Proceedings of the 11th International Symposium on Materials in Space Environment*, Aix-en-Provence (France), Sept. 2010.

D. Edwards
Associate Editor